A 3D track finder for the Belle II CDC L1 trigger

Sebastian Skambraks[1], Steffen Bähr[2], Jürgen Becker[2], Christian Kiesling[1], Sara McCarney[1], Felix Meggendorfer[1], Raynette van Tonder[2] and Kai Lukas Unger[2]

1 Max Planck Institute for Physics, Föhringer Ring 6, 80805 Munich, Germany
2 Karlsruhe Institute of Technology, Kaiserstraße 12, 76131 Karlsruhe, Germany

E-mail: sskambra@mpp.mpg.de

Abstract. Machine learning methods are integrated into the pipelined first level (L1) track trigger of the upgraded flavor physics experiment Belle II at KEK in Tsukuba, Japan. The novel triggering techniques cope with the severe background from events outside the small collision region provided by the new SuperKEKB asymmetric-energy electron-positron collider. Using the precise drift-time information of the central drift chamber which provides axial and stereo wire layers, a neural network L1 trigger estimates the 3D track parameters of tracks, based on input from the axial wire planes provided by a 2D track finder. An extension of this 2D Hough track finder to a 3D finder is proposed, where the single hit representations in the Hough plane are trained using Monte Carlo. This 3D finder improves the track finding efficiency by including the stereo sense wires as input. The estimated polar track angle allows a specialization of the subsequent neural networks to sectors in the polar angle.

1. Introduction

Belle II is the new flavor physics detector at the high luminosity B factory SuperKEKB in Tsukuba, Japan [1]. In the presently running Phase 3 of SuperKEKB (spring 2019), the first physics collisions are recorded with the full detector geometry installed. The asymmetric e^+e^- collider is operated at the $\Upsilon(4S)$ resonance, with beam energies of $E(e^+) = 4\,\text{GeV}$ and $E(e^-) = 7\,\text{GeV}$. Belle II allows to perform precision tests of the Standard Model (SM) of particle physics, as well as searches for physics beyond the SM (BSM). Besides the typical $B\bar{B}$ events with an average momentum of 500 MeV per track and an average track multiplicity of 11 tracks per event, there are also many low multiplicity channels that are important in searches for BSM physics, like searches for dark matter or lepton flavor violation processes. In addition, low multiplicity hadronic events at low center-of-mass energies, resulting from initial state radiation, may offer a handle to improve the hadronic loop corrections in the $g-2$ analysis.

The luminosity upgrade that is inherently connected with an increase of the background rate poses a challenge for the trigger system. As determined from background simulations and the observed background in the early Belle II data, a large fraction of background tracks are seen along the longitudinal axis z outside of the interaction region. The expected background z distribution at Belle II and the observed distribution from the early Phase 3 data of Belle II are shown in Figure 1 [2]. A large proportion of these background tracks are backscattered particles produced from interactions of the primary particles with the detector material [2]. The addition of a z vertex trigger enables a significant reduction of the background track rate and allows to relax other trigger conditions, which could give access to low multiplicity events. Following a

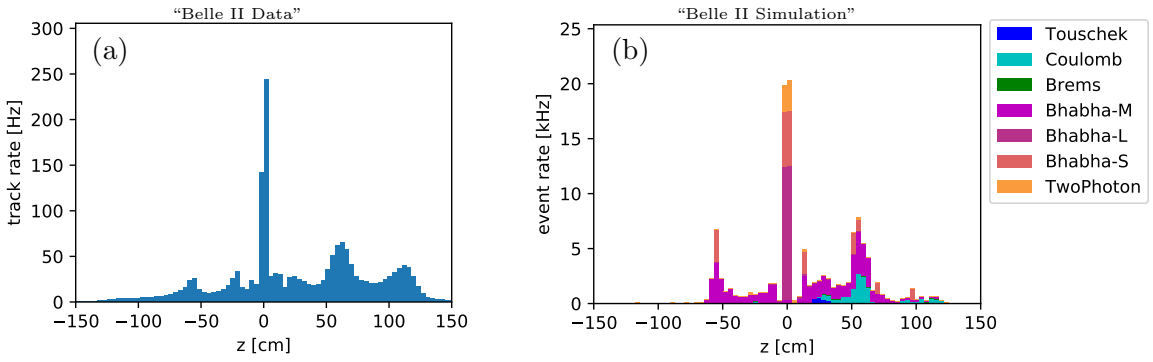

Figure 1. (a) Observed z distribution of reconstructed tracks from an early run of Belle II (exp 7, run 4048). (b) Simulated distribution of the z vertex positions of background tracks found by the 2D track finder for different background types (luminosity and machine) [2]. The luminosity in (a) is $\approx 500\times$ lower than the design luminosity of Belle II ($\mathcal{L} = 8 \times 10^{35}\,\mathrm{cm}^{-2}\,\mathrm{s}^{-1}$), which was used in the idealized Belle II background-only simulation (b).

track finder based on a 2D Hough transformation [3], the single track z vertex reconstruction at the first level (L1) trigger is realized by two methods: a neural network [4, 5, 6, 7] and in parallel by a least square fitter [8]. Here, a possible 3D upgrade for the track finder is introduced. Such an upgrade would improve the track finding efficiency, and provide additional a priori information for a better accuracy of the 3D track reconstruction methods.

2. CDC L1 Trigger

The Belle II L1 trigger is a pipelined hardware trigger mainly composed of subtriggers derived from the drift chamber and the electromagnetic calorimeter, and a global decision logic, where the subtrigger results are combined to issue the trigger signal. The requirements for the Belle II L1 trigger are a maximum trigger rate of 30 kHz within a maximum latency of 5 µs and with a pipeline clocked every 32 ns [1, 9]. To fulfill these requirements, all subtriggers are implemented in hardware, based on FPGA technology, which provides a high degree of parallel and deterministic computation to achieve the required timing performance. Additionally, this technology offers a sufficient number of High-Speed Input/Output resources to fulfill the bandwidth and connectivity requirements.

The central drift chamber (CDC) is the only tracking detector at the L1 trigger. It contains 14336 sense wires arranged in 56 cylindrical layers around the z axis, which are combined into 9 superlayers (SLs) with the same orientation: wires in the axial SLs are aligned parallel to the z axis, while the inclined stereo SLs have different stereo angles with respect to the z axis that allow for a 3D track reconstruction. The tracking accuracy is determined by the measurement of the drift-times at the sense wires.

In a first noise suppression and data reduction step, the wire hits are combined into track segments (TSs) in the 9 SLs by searching for a hourglass shaped pattern of wires in close proximity [1, 9]. Each of the 2336 TSs provides the position of a single priority wire within the TS pattern, the drift-time measured at this priority wire and a left/right information based on the wire hit pattern within the TS. The TSs are the input to the 2D track finder, the event time finder, the 3D fitter and the neural network trigger. The present 2D track finder uses only the axial hit positions (without drift-time) as input to find 2D track candidates (p_T, ϕ) with a circular 2D Hough transformation. For each found track, a neural network and the fitter use the

Table 1. Binning of the track and hit parameters in the array A; p_T is the transverse momentum, ϕ is the azimuthal and θ the polar angle of the track; *id* is the unique identification number of a TS hit in the CDC trigger; *prio* is the position of a single selected reference wire within the TS - the priority wire. In the predefined shape of a TS, three wires are possible candidates for this priority wire.

	p_T	ϕ	θ	*id*	*prio*
bins	40	384	9	2336	3

full TS information (including the drift-times) to provide precise 3D track estimates. In order to improve the accuracy in the cases where stereo TSs are missing, the neural network trigger has a set of 5 expert networks pretrained to missing stereo TSs.

3. 3D Track Finder

The 2D track finder uses only the axial TSs as input, as they appear as points in the transverse plane. If stereo TSs were included in a 3D track finder, the track finding efficiency could be improved. However, the model must be extended to a 3D Hough plane, since stereo wires appear as short line segments in the 2D transverse plane. By extending the Hough space to 3D, an additional 3D track parameter can be estimated. This is particularly beneficial for the neural network trigger, where a priori knowledge of the track can be used to sectorize the input in order to train expert networks for these sectors.

Due to the magnetic field of 1.5 T, tracks can be described by circles in the transverse plane. In the circular 2D Hough transformation, the hit points in real space are transformed to sine curves in parameter space. The track parameters are then found at the intersections of the hit curves [6]. In hardware, a binned Hough space is used: after summing up the single hit contributions, the tracks are identified by a peak finding algorithm.

3.1. Model

The model for a 3D track finder is motivated by the Bayes estimation of conditional probabilities for the random variables T (set of tracks) and H (set of hits):

$$P(T|H) = \frac{P(H|T)P(T)}{P(H)} \tag{1}$$

where $P(T|H)$ is the probability for a set of tracks T given a set of hits H [5]. In a binned track parameter space, an array can be identified of probabilities $P(t|H)$ for each possible track t to be built out of the set of observed hits $h \in H$. With a peak finding algorithm, tracks can be identified as local maxima in the probability distribution. This is a very general approach that allows an easy change of the track and hit parametrization. By choosing the same track and hit parametrization as in the 2D track finder, equivalent results are obtained.

In the 3D finder, the hit contributions to the probabilities in the track parameter space are represented by a 5D array $A[t,h] \propto P(t|h)$. The tracks are parametrized by p_T^{-1}, ϕ and θ, while the hits by their *id* and *prio* (priority position). For tracks associated to a vertex at the IP, p_T^{-1} is the inverse transverse momentum which is proportional to the curvature of the track; ϕ and θ are the azimuthal and polar angles of the track momentum at the IP. While stereo hits appear as line segments in a transverse 2D plane, the binning in the track parameter θ allows to represent the stereo hits as points in each θ bin. The used binning is shown in Table 1.

Table 2. Track parameter ranges of the simulated single $\mu^{\pm}$ tracks used for the tests: (a) tracks in the full acceptance region of the CDC; (b) flatter polar angle θ and lower transverse momentum p_T where not all layers of the CDC might get a hit.

	p_T [GeV]	ϕ [°]	z [cm]	θ [°]
(a)	$[0.35, 7]$	360	$[-1, 1]$	$[35, 123]$
(b)	$[0.2, 7]$	360	$[-1, 1]$	$[19, 140]$

The quantity A is trained on $2.5 \cdot 10^5$ Monte Carlo simulated single $\mu^{\pm}$ tracks associated to vertices at the IP and the track parameters within the ranges listed in Table 2. For each track in the training run, the related hits are selected, a binning is applied to the track parameters and the array $A[t, h]$ is incremented for all (track, hit) pairs. After the array is filled, it is normalized to make all tracks equally probable.

$$A[t, h] = \frac{A[t, h]}{\sum_{\text{all } h} A[t, h]} \tag{2}$$

Note that this sum is taken over the set of all possible hits for each track. In the end, a bit width of 3 bits is applied to the weights in A, with the effect that a single hit can contribute to a track with a maximum weight of 2^3.

After A is trained, it can be used for track finding. The Hough space $B[t]$ is constructed by summing up all single hit contributions h of the set of observed hits ($h \in H$) in the event:

$$B[t] = \sum_{h \in H} A[t, h] \tag{3}$$

With this summation, $B[t]$ cannot be interpreted as a probability, but as a weight with which the hits contribute to each possible track. The local maxima are preserved such that peaks in $B[t]$ identify the most probable tracks in the event.

A variation of the density-based clustering algorithm DBSCAN [10] is used to find connected regions of cells with `minweight` $= 24$ in $B[t]$. Once the cluster candidates are found, cells with a weight less than 85 % of the peak weight within the clusters are removed. A confusion matrix of the hit to cluster relations is used to assign the hits to the clusters where they contribute with the largest weight. Cluster candidates with less than `minhits` $= 4$ assigned hits are removed and the hits are reassigned to bigger clusters. From the found clusters, the track parameters are calculated as the weighted mean of the cluster cells.

3.2. Results

The accuracy of the found track parameters and the efficiency for the track finding are analyzed with Monte Carlo events in two different track parameter ranges (see Table 2). The results of the 3D finder are compared to the existing 2D finder.

Figure 2 shows the accuracies in a test run with the track parameter range (a) (see Table 2), where tracks from the IP can produce hits in all SLs. In both 2D track parameters (p_T, ϕ), the 3D finder has an improved accuracy. In addition, it provides a θ estimate with $\Delta\theta \approx 3°$, which is better than the θ bin width in A. This is possible since the track parameters are calculated as the weighted mean of the contributing cluster cells. There is no significant difference in the recognized charges of the tracks.

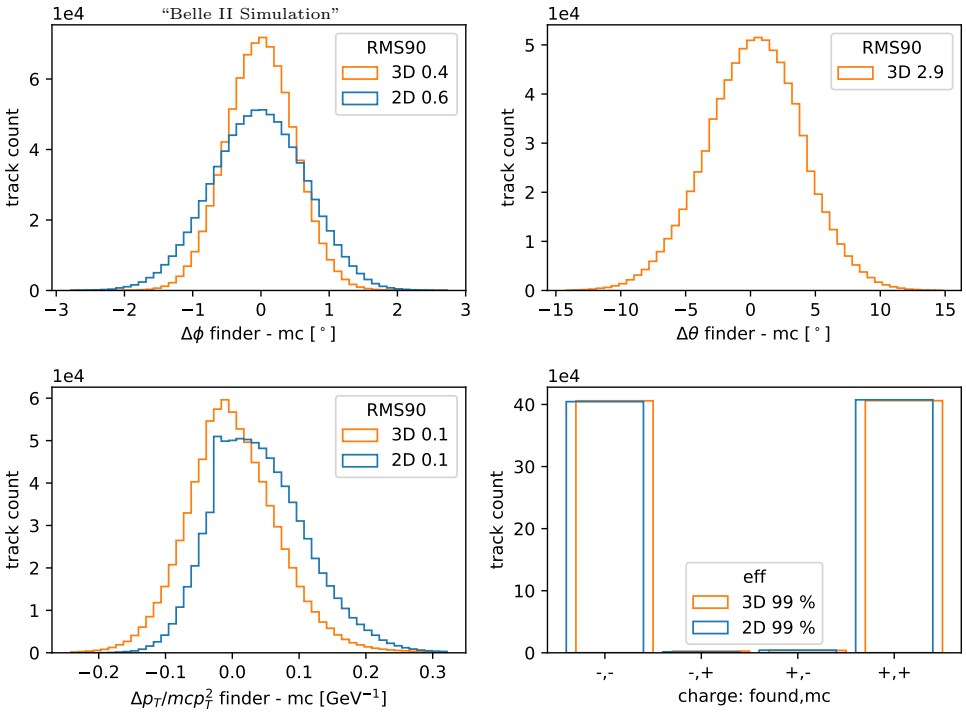

Figure 2. Accuracy of the found track parameters with the 3D track finder in comparison to the 2D track finder. The track parameter ranges (a) of Table 2 are used.

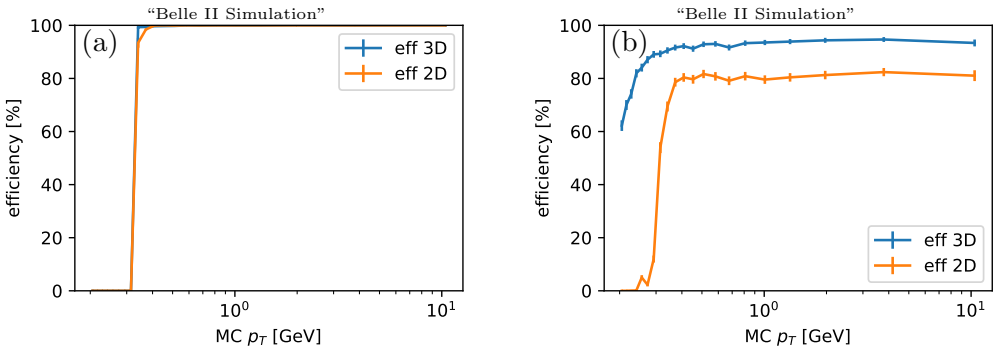

Figure 3. (a) Track finding efficiency for tracks within the full detector acceptance region, where tracks pass through all SLs of the CDC. (b) Track finding efficiency for tracks with a flatter polar angle θ, where not all SLs of the CDC might get a hit.

Figure 3 shows the p_T dependent track finding efficiency for both track parameter ranges. In Figure 3 (a) the track parameter range (a) of Table 2 is used. Both finders achieve an efficiency of $\approx 100\,\%$ in the high p_T region. Only in the low p_T region the 3D finder has an improved track finding efficiency. Figure 3 (b) shows the efficiency for the track parameter range (b) of Table 2. It contains tracks with lower transverse momentum p_T and flatter θ angles. For the finders, it is more difficult to reconstruct such tracks, as not all SLs might get a hit. The 3D finder shows a significantly improved track finding efficiency in all p_T regions.

4. Conclusion and Outlook

An improvement of the estimated track parameter accuracy and the track finding efficiency with a 3D finder has been measured in a test setup with simulated single tracks. While the 2D finder already reaches almost 100 % efficiency for tracks within the full CDC acceptance regions where tracks have hits in all SLs, a significant improvement can be achieved for tracks with lower p_T and flatter θ where not all tracks have hits in all SLs. The estimated θ, with an accuracy of $\Delta\theta \approx 3^\circ$, could be used as an additional input to the 3D track reconstruction, e.g., by a training a pool of expert neural networks for the θ sectors. The 3D finder will be a useful replacement of the 2D finder: for tracks in the full CDC acceptance region, both methods achieve equivalent efficiencies while a significant efficiency improvement can be achieved for tracks at the boundaries of the acceptance region. The presented method is carried out in a simulation framework and follow-up studies on the realization in hardware are necessary. The generality of this 3D finder makes it interesting also in offline tracking applications where two consecutive 2D track finding steps can be combined into a single 3D step. At Belle II, this method might also be useful in the track finding with the double-sided silicon strip vertex detector, where presently a 2D track finder in the transverse plane is followed by a 2D track finder in the longitudinal plane: using the 3D track parameter θ in a single 3D finder could reduce the large number of fake tracks from combinatorial effects in the second longitudinal 2D finder step.

References

[1] Abe T *et al.* 2010 *ArXiv e-prints* (*Preprint* 1011.0352) http://arxiv.org/abs/1011.0352

[2] Skambraks S, Neuhaus S and Kiesling C 2018 *Journal of Physics: Conference Series* **1085** 042026 http://stacks.iop.org/1742-6596/1085/i=4/a=042026

[3] Hough P V C 1959 *HEACC, Proc. 2nd Int. Conf. on High-Energy Accelerators and Instrumentation* vol C590914 pp 554–558 http://inspirehep.net/record/919922/files/HEACC59_598-602.pdf

[4] Neuhaus S, Skambraks S, Abudinen F, Chen Y, Feindt M, Frhwirth R, Heck M, Kiesling C, Knoll A, Paul S and Schieck J 2015 *Journal of Physics: Conference Series* **608** 012052 http://stacks.iop.org/1742-6596/608/i=1/a=012052

[5] Skambraks S, Neuhaus S and Kiesling C 2016 *EPJ Web of Conferences* vol 127 (EDP Sciences) p 00016

[6] Neuhaus S, Skambraks S and Kiesling C 2017 *EPJ Web of Conferences* vol 150 (EDP Sciences) p 00009

[7] Baehr S, Skambraks S, Neuhaus S, Kiesling C and Becker J 2017 *Journal of Instrumentation* **12** C03065 http://stacks.iop.org/1748-0221/12/i=03/a=C03065

[8] Won E, Kim J and Ko B 2018 *Journal of the Korean Physical Society* **72** 33–37

[9] Iwasaki Y, Cheon B, Won E, Gao X, Macchiarulo L, Nishimura K and Varner G 2011 *Nuclear Science, IEEE Transactions on* **58** 1807–1815 ISSN 0018-9499

[10] Ester M, Kriegel H P, Sander J, Xu X *et al.* 1996 *Kdd* vol 96 pp 226–231